



Secondary ion emission enhancement assisted by electron beam in secondary ion mass spectrometry

Wei-Chiang Lee, J. Hwang*

Department of Materials Science and Engineering, National Tsing Hua University, Hsin-Chu City, 101, Section 2, Kuang-Fu Road, Hsinchu 30013, Taiwan, ROC

ARTICLE INFO

Article history:

Received 13 February 2008

Received in revised form 15 April 2008

Accepted 21 April 2008

Available online 2 May 2008

Keywords:

Secondary ion mass spectrometry

Ion–solid interaction

Electron stimulated desorption

Penning ionization

Energy spectrum

ABSTRACT

Secondary ion emission was enhanced by electron beam in a typical secondary ion mass spectrometry (SIMS) operation, which was demonstrated using the shallow p/n junction implanted with BF_2^+ ions of a dosage of $2.3 \times 10^{15} \text{ cm}^{-2}$ at 20 keV. In the SIMS mass spectra measurements, the $^{19}\text{F}^+$ signal is enhanced by 39 times at an electron beam current of $100 \mu\text{A}$. In contrast, the $^{11}\text{B}^+$ signal is slightly enhanced by a factor of $\sim 50\%$. In order to characterize the spatial distribution of secondary ions along the surface normal direction, the energy spectra of $^{19}\text{F}^+$, $^{11}\text{B}^+$ and $^{30}\text{Si}^+$ ions were measured by altering the sample potential by $\pm 50\text{V}$ (relative the original sample bias 2 kV). The energy spectra reveal that most $^{19}\text{F}^+$ ion signal is generated by electron beam stimulated desorption on the sample surface and some by the electron induced post-ionization in the gas phase above the sample surface. In contrast, only small enhancements of $^{11}\text{B}^+$ and $^{30}\text{Si}^+$ occur on the sample surface. No $^{11}\text{B}^+$ and $^{30}\text{Si}^+$ ions are generated in the gas phase above the sample surface. The enhancement of $^{11}\text{B}^+$ increases linearly with electron beam current based on the depth profile data of $^{11}\text{B}^+$. This supports the occurrence of Penning ionization for $^{11}\text{B}^+$ on the sample surface. The ionization enhancement of $^{11}\text{B}^+$ is dominated by oxygen radicals O_2^+ .

© 2008 Elsevier B.V. All rights reserved.

1. Introduction

Secondary ion mass spectrometry (SIMS) has attracted much attention in the electronic industry due to the ultra-low detection limit. SIMS is currently the most appropriate tool to measure the depth profiles of dopants in electronic devices. The sensitivity of SIMS is directly correlated to the secondary ion emission yields of chemical elements that are usually enhanced by optimizing instrumental parameters such as primary beam species, primary beam energy, and angle of incidence. In order to further enhance SIMS sensitivity, other techniques such as post-acceleration, post-ionization and gas flooding have been investigated. Post-acceleration is applied to accelerate secondary ions to increase the count rate especially in the regime of low ion energy.[1] Post-ionization is used in the Secondary Neutral Mass Spectrometry (SNMS) to ionize neutrals sputtered out of the sample surface by electrons [2] or laser [3–7] such that secondary ion yields are enhanced. Gas flooding is performed by leaking a gas (O_2 , CF_3 , CF_2Cl_2 or CCl_4) to the sample surface during primary ion beam bombardment. The positive secondary ion emission yields are enhanced by chemical reactions because oxygen, fluorine or chlorine tends

to form strong ion bonds by taking electrons out of matrix atoms [8–10].

In this paper, the concept of post-ionization is applied to enhance the SIMS sensitivity by the assistance of electron beam. The electron beam, emitted from the electron gun that is usually equipped for charging neutralization, is incident directly onto the sample surface during the O_2^+ ion bombardment in a SIMS operation. The $^{11}\text{B}^+$, $^{19}\text{F}^+$ and $^{30}\text{Si}^+$ ions are chosen to illustrate the electron beam assisted ionization of the shallow p/n junction implanted with BF_2^+ ions of a dosage of $2.3 \times 10^{15} \text{ cm}^{-2}$ at 20 keV. The dependence of ionization enhancement on chemical species and related mechanisms will be addressed.

2. Experimental procedures

A P-type Si(100) wafer was implanted with BF_2^+ ions at 20 keV with a dosage of $2.3 \times 10^{15} \text{ cm}^{-2}$. The as-implanted p-Si(100) wafer was fed into a magnetic sector mass spectrometer (CAMECA IMS-6f) in which an electron gun was equipped originally for charge neutralization. The electron gun was tuned to supply energetic electrons that were able to enhance the ionization yield during the SIMS measurements. In order to eliminate the knock-on effect, the primary impact energy, i.e., the energy of O_2^+ ions was kept at 2 keV that is approximately one half of the boron effective energy for the implantation of BF_2^+ ions at 20 keV [11–13].

* Corresponding author.

E-mail address: jch@mx.nthu.edu.tw (J. Hwang).

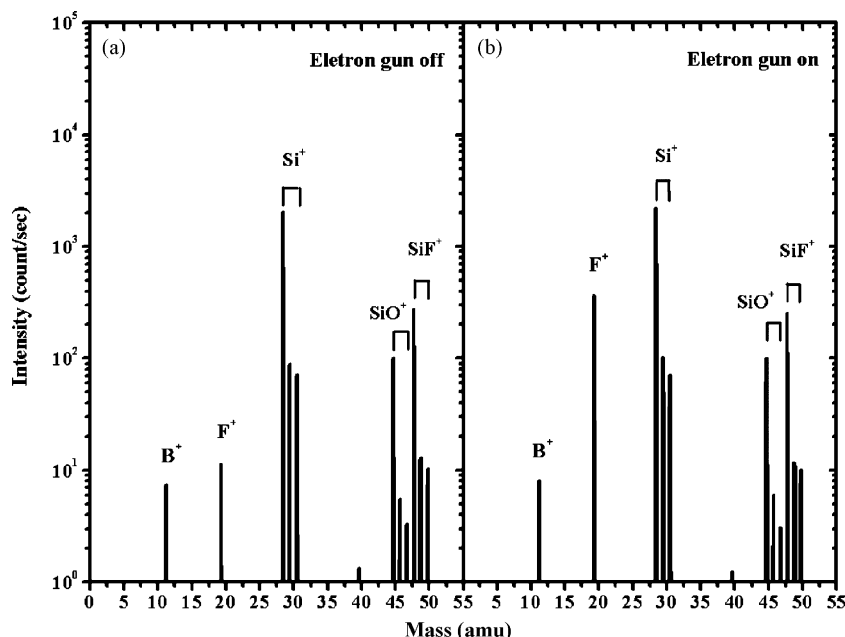


Fig. 1. Mass spectra of the shallow p/n junction implanted with BF_2^+ at 20 keV with a dosage of $2.3 \times 10^{15} \text{ cm}^{-2}$. (a) Electron gun off. (b) Electron gun on.

The O_2^+ ion energy was set at 4 keV and the sample was biased at 2 kV in order to keep the incident angle of the O_2^+ primary ions around 45° from surface normal [14,15]. All the mass spectra were taken at a raster area of $250 \mu\text{m} \times 250 \mu\text{m}$ at $\sim 35 \text{ nA}$. The secondary ions were collected from a circular area of $40 \mu\text{m}$ in diameter within the raster area. In the depth profile measurements, the primary O_2^+ ion beam was scanned across a raster area of $150 \mu\text{m} \times 150 \mu\text{m}$ at $\sim 35 \text{ nA}$. The electron gun was biased at -4.5 kV such that the energy of electrons was 6.5 keV relative to the sample. The electron beam current varying from 0 to $180 \mu\text{A}$ was incident normally onto the sample surface in the depth profiling. A series of $^{11}\text{B}^+$ depth profiles were taken to characterize the enhancement of ionization efficiency by the assistance of electron beam.

In order to characterize the spatial distribution of secondary ions along the surface normal direction, the energy spectra of $^{19}\text{F}^+$, $^{11}\text{B}^+$ and $^{30}\text{Si}^+$ ions were measured by altering the sample potential $\pm 50 \text{ V}$ relative to the original sample bias (2 kV). In order to

improve the accuracy of energy distribution of sputtered ions in the SIMS measurements, a smaller field aperture ($75 \mu\text{m}$) in the extraction electrode was selected in order to obtain a smaller acceptance angle such that the energy dispersion of ions after acceleration in the electric field can be reduced. The sample bias was lowered from 4.5 kV (normal value) to 2 kV . The secondary Si^+ ions of high intensity were used to calibrate the origin of ion energy in the energy spectra. The ion energy passing through electrostatic sector analyzer (ESA) was set to 2 kV and the resolution of ion pass energy was $\sim 5.5 \text{ eV}$. The energy-selective slit following the ESA was moved to an optimum position to maximize the intensity of Si^+ ions at a sample bias of 2 kV . The low energy edge of the energy spectrum of Si^+ ions was then set to 0 eV . At this condition, the “negative” energy in the energy spectra characterizes the initial kinetic energy of ions on the surface. The “positive” energy in the energy spectra characterizes the spatial position of the ions generated above the surface since a uniform electric field is constructed between the extraction electrode (0 V) and the sample (2 kV) [16].

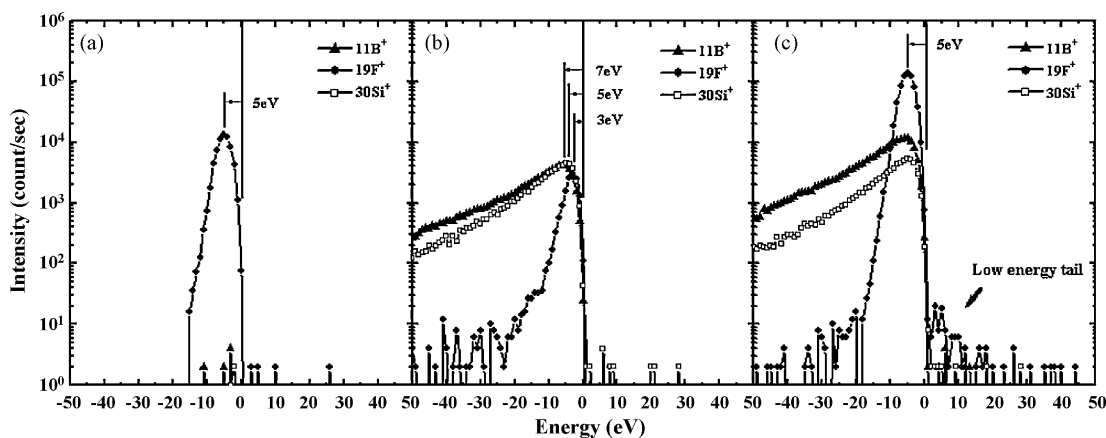


Fig. 2. Energy spectra of $^{11}\text{B}^+$, $^{19}\text{F}^+$ and $^{30}\text{Si}^+$ from the BF_2^+ implanted silicon wafer under different bombardment conditions: (a) electron bombardment, (b) O_2^+ bombardment, and (c) simultaneous O_2^+ and electron bombardment. The electron bombardment is operated at 6.5 kV and $37 \mu\text{A}$. The O_2^+ bombardment is operated at 2 keV and 24 nA .

3. Results and discussion

3.1. Mass spectra under O_2^+ and O_2^+ plus electron bombardment

Fig. 1(a) and (b) illustrate the $^{11}B^+$ ion mass spectra of the shallow p/n junction implanted with BF_2^+ ions of a dosage of $2.3 \times 10^{15} \text{ cm}^{-2}$ at 20 keV in a typical SIMS operation with electron gun off and on, respectively. During the mass spectra detection, the raster size is tuned to a larger size of $250 \mu\text{m} \times 250 \mu\text{m}$ in order to reduce the sputtering rate such that all the extracted signals are approximately from the same depth inside the implanted sample. The $^{19}F^+$ signal is enhanced by 39 times at an electron beam current of $100 \mu\text{A}$, which is the most enhanced ion signal with electron gun on. In contrast, the $^{11}B^+$ signal is slightly enhanced by a factor of $\sim 30\%$. The $^{19}F^+$ enhancement in Fig. 1(b) is a well known result, which has been attributed to the electron stimulated desorption process [17,18], illustrated by Lanzillotto and Magee in 1990.

3.2. Energy spectra under electron, O_2^+ , and O_2^+ plus electron bombardment

Fig. 2(a)–(c) show the energy spectra of $^{11}B^+$, $^{19}F^+$ and $^{30}Si^+$ obtained under different bombardment conditions: electron bombardment [Fig. 2(a)], O_2^+ bombardment [Fig. 2(b)] and simultaneous O_2^+ and electron bombardments [Fig. 2(c)]. With electron gun on only, a prominent $^{19}F^+$ signal appears in the energy spectra in Fig. 2(a). This confirms that the occurrence of the enhancement of $^{19}F^+$ by electron stimulated desorption. From a chemical perspective, a surface energy barrier exists for fluorine atoms before desorption to occur. Note that the maximum peak of $^{19}F^+$ occurs at -5 eV in Fig. 2(a), indicating that most $^{19}F^+$ ions right after desorption on the surface exhibit a kinetic energy of 5 eV . The kinetic energy plays a role for $^{19}F^+$ ions to overcome surface energy barrier and to escape from the sample. In a typical SIMS operation with O_2^+ bombardment on only, $^{19}F^+$ ions exhibit narrower energy distribution than $^{11}B^+$ and $^{30}Si^+$ ions. The maximum peaks of $^{11}B^+$, $^{19}F^+$ and $^{30}Si^+$ ions appear at different “negative” energy positions, as shown in Fig. 2(b). The energy required to overcome surface energy barrier is 7 eV for $^{11}B^+$, 5 eV for $^{30}Si^+$, and 3 eV for $^{19}F^+$ ions based on the maximum peak positions. When the electron gun is turned on during O_2^+ bombardment, two new features appear in the energy spectra in Fig. 2(c) due to the electron beam interaction. First, the maximum position of the $^{19}F^+$ signal is back to -5 eV and is greatly increased by ~ 45 times. According to the result in Fig. 2(a), the maximum peak of $^{19}F^+$ ions appears at -5 eV for electron stimulated desorption. The great enhancement of $^{19}F^+$ at the origin is thus attributed to electron stimulated desorption on the sample surface. This supports that electron stimulated desorption dominates the excitation process of $^{19}F^+$. Second, a low energy tail of $^{19}F^+$ appears on the positive energy side in Fig. 2(c). The low energy tail, which characterizes the intensity of ions at a position above the sample surface, indicates that only $^{19}F^+$, rather than $^{11}B^+$ and $^{30}Si^+$, ions can be generated in the gas phase above the sample surface. Very probably some quasi-molecules (e.g., SiF^+) sputtered out of the sample are further ionized by the assistance of electron beam, which play a role in the ion enhancement of $^{19}F^+$ [19]. The ionization of fluorine neutral atoms in the gas phase above the sample surface is excluded since the ionization potential of fluorine is higher than that of boron and silicon. With regard to the enhancement of $^{19}F^+$ in Fig. 1(b), most ion signal is generated by electron beam stimulated desorption on the sample surface and some by the post-ionization of electron beam to form the low energy tail from gas phase in Fig. 2(c).

Note that no $^{11}B^+$ and $^{30}Si^+$ ion signals appear in the low energy tail in Fig. 2(c), equivalent to no $^{11}B^+$ and $^{30}Si^+$ ions generated from

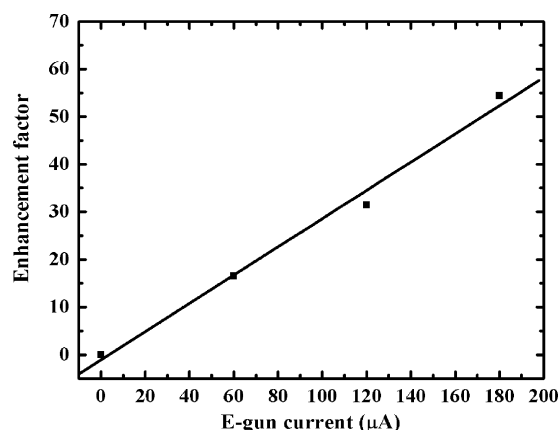


Fig. 3. Linear plot of the $^{11}B^+$ depth profile in a shallow p/n junction implanted with BF_2^+ at 20 keV with a dosage of $2.3E15 \text{ cm}^{-2}$. The electron beam energy is 6.5 keV relative to the Si sample.

the neutral atoms (gas phase) above the sample surface. Moreover, $^{11}B^+$ and $^{30}Si^+$ ion signals slightly increase in intensity in Fig. 2(c). The slight enhancement of $^{11}B^+$ and $^{30}Si^+$ in the mass spectra in Fig. 1(b) is thus attributed to the ionization on the sample surface.

3.3. In-depth analysis under O_2^+ and O_2^+ plus electron bombardment

The slight enhancement of $^{11}B^+$ in Figs. 1(b) and 2(c) is proposed as Penning ionization on the sample surface based on the depth profile data. Fig. 3 shows the linear plot of the $^{11}B^+$ depth profile for the shallow p/n junction implanted with BF_2^+ ions of a dosage of $2.3 \times 10^{15} \text{ cm}^{-2}$ at 20 keV under different electron beam current conditions. Two major features appear and are described as follows. First, the depth profile of the $^{11}B^+$ signal exhibits a traditional implantation shape. Second, the $^{11}B^+$ signal increases linearly with electron beam current. The increase of the $^{11}B^+$ signal can be quantified by the enhancement factor e (%) that is defined as:

$$e = \frac{h_1 - h_2}{h_2} \times 100\%$$

where h_1 is the enhanced signal with electron gun on and h_2 is the signal with electron gun off [20]. The enhancement factor of the $^{11}B^+$ signal increases linearly with electron beam current, as shown in Fig. 4. The enhancement factor increases up to 53% at an electron beam current of $180 \mu\text{A}$.

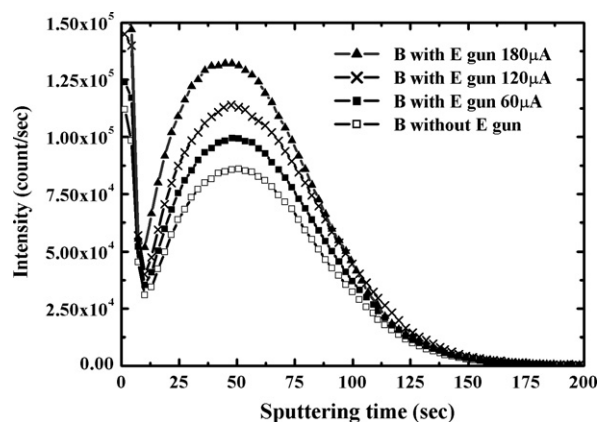


Fig. 4. Enhancement factor for the $^{11}B^+$ signal as a function of electron beam current in the electron beam assisted ionization process.

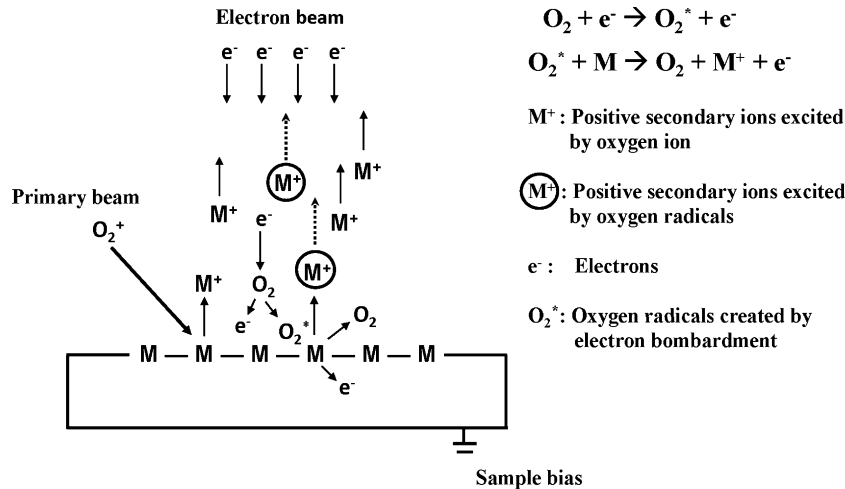


Fig. 5. Schematic diagram showing the ionization of $^{11}\text{B}^+$ by the Penning ionization mechanism induced by electron beam.

Based on the data in Fig. 2(b), only fluorine can be ionized on and above the sample surface by electron beam. The ionization of $^{11}\text{B}^+$ directly by electron beam does not occur based on the energy spectra in Fig. 2(a). The most probable reaction for electron beam is to excite neutral atoms to their radical states in the gas phase and on the sample surface during the incidence of electrons onto the sample surface. O_2 is considered as the most probable neutral atoms in the gas phase generated by the primary O_2^+ ions in a SIMS chamber based on two reasons. First, the re-sputtered oxygen can be in the form of O , O_2 and O^- where the O^- ions cannot escaped from the sample surface since the sample is biased at 2 kV. Second, the lifetime of O_2 is much longer than O [21–24].

Considering the interaction among O_2 , matrix atom (M) and electron beam (e^-), electron beam can excite O_2 into O_2^* radicals and matrix atoms into M^* radicals according to Eqs. (1) and (2) below.



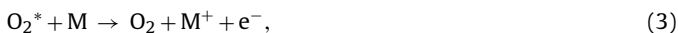
The reaction rate r_1 and r_2 are, respectively, expressed as

$$r_1 = \frac{d[\text{O}_2^*]}{dt} = k_1[\text{O}_2][\text{e}^-]$$

$$r_2 = \frac{d[\text{M}^*]}{dt} = k_2[\text{M}][\text{e}^-]$$

The generation rate of O_2^* and M^* radicals, i.e., $d[\text{O}_2^*]/dt$ and $d[\text{M}^*]/dt$, are proportional to electron beam current $[\text{e}^-]$.

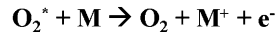
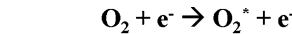
The Penning ionization can well explain the depth profile data of $^{11}\text{B}^+$ in Fig. 3. The Penning ionization characterizes the reaction involving O_2^* radicals, which is sketched in Fig. 5 and is described in the Eq. (3).



where O_2^* denotes the oxygen radical, M the matrix atom, O_2 the oxygen molecule, M^+ the ion from matrix, and e^- the electron. The reaction rate r_3 in the Eq. (3) is expressed as

$$r_3 = \frac{d[\text{M}^+]}{dt} = k_3[\text{O}_2^*][\text{M}]$$

The generation of M^+ ion is proportional to the concentration of O_2^* . Taking into account the Eqs. (1) and (3), the generation of M^+ ion is proportional to electron beam current $[\text{e}^-]$. This is in good agreement with the depth profile data of $^{11}\text{B}^+$ in Fig. 3.



M^+ : Positive secondary ions excited by oxygen ion

M^* : Positive secondary ions excited by oxygen radicals

e^- : Electrons

O_2^* : Oxygen radicals created by electron bombardment

The other ionization process involving M^* radicals is described below [25,26].



The reaction rate r_4 is expressed as

$$r_4 = \frac{d[\text{M}^+]}{dt} = k_4[\text{M}^*]^2$$

The generation of M^+ ion is proportional to $[\text{M}^*]^2$, equivalent to $[\text{e}^-]^2$.

Taking into account the Eqs. (2) and (4), the generation of M^+ ion is proportional to electron beam current $[\text{e}^-]^2$. The ionization process involving M^* radicals is thus excluded since the enhancement of $^{11}\text{B}^+$ in Fig. 4 is proportional to $[\text{e}^-]$.

The role of oxygen in the Penning ionization process is further supported by the following experiment. In a SIMS operation, the O_2^+ primary ions are replaced by Cs^+ ions in the $^{11}\text{B}^+$ depth profile measurements for the shallow p/n junction implanted with BF_2^+ ions. No enhancement of ionization efficiency of $^{11}\text{B}^+$ was observed. This supports the role of oxygen in the Penning ionization process for the ionization enhancement.

4. Conclusion

The secondary ion emission enhancement by electron beam has been illustrated for the shallow p/n junction implanted with BF_2^+ ions of a dosage of $2.3 \times 10^{15} \text{ cm}^{-2}$ at 20 keV in a typical SIMS operation. The ionization enhancement depends on the type of ion species. Most $^{19}\text{F}^+$ ion signal is generated by electron beam stimulated desorption on the sample surface and some by the electron induced post-ionization in the gas phase above the sample surface. In contrast, only small enhancements of $^{11}\text{B}^+$ and $^{30}\text{Si}^+$ occur on the sample surface. No $^{11}\text{B}^+$ and $^{30}\text{Si}^+$ ions are generated in the gas phase above the sample surface. The enhancement of $^{11}\text{B}^+$ increases with electron beam current, which is attributed to the Penning ionization on the sample surface.

Acknowledgements

The authors would like to thank Mr. Z.-C. Lue (CAMECA Taiwan Co., Ltd.), Dr. Alexandre Merkulov and Dr. Paula Peres (CAMECA France Co., Ltd.) for helpful advices in tuning the electron gun. The valuable discussions with Dr. S. Biswas and Dr. Christopher Mulcahy (Cascade Scientific Ltd.) are also appreciated.

References

- [1] R. Liu, C.M. Ng, A.T.S. Wee, Ultra shallow secondary ion mass spectrometry. Solid-State and Integrated-Circuit Technology, 2001, ieeexplore.ieee.org.
- [2] R. Jede, H. Peters, G. Dunneber, O. Ganschow, U. Kaiser, K. Seifert, Quantitative depth profile and bulk analysis with high dynamic range by electron gas sputtered neutral mass spectrometry, *J. Vac. Sci. Technol. A* 6 (1988) 2271.
- [3] Gunther K. Nicolussi, Michael J. Pellin, Keith R. Lykke, Jennifer L. Trevor, Donald E. Mencer, Andrew M. Davis, Surface analysis by SNMS: femtosecond laser postionization of sputtered and laser desorbed atoms, *Surf. Interface Anal.* 24 (1996) 363.
- [4] Wolfgang Husinsky, Gerhard Betz, Fundamental aspects of SNMS for thin film characterization: experimental studies and computer simulations, *Thin Solid Films* 272 (1996) 289.
- [5] H. Oechsner, Analysis of electrically non-conducting sample structures with electron and mass spectroscopic methods, *Thin Solid Films* 341 (1999) 105.
- [6] Y. Higashi, Quantitative depth profiling by laser-ionization sputtered neutral mass spectrometry, *Spectrochim. Acta Part B* 54 (1999) 109.
- [7] H. Shichi, S. Osabe, M. Sugaya, T. Ino, H. Kakibayashi, K. Kanehori, Y. Mitsui, A resonance photoionization sputtered neutral mass spectrometry instrument for submicron microarea analysis of ULSI devices, *Appl. Surf. Sci.* 203–204 (2003) 228.
- [8] A. Benninghoven, F.G. Rudenauer, H. Werner, Secondary Ion Mass Spectrometry: Basic Concepts, Instrumental Aspects, Applications and Trends, John Wiley & Sons, New York, 1987.
- [9] W. Reuter, Secondary ion emission from metal targets under carbon trifluoride ion (CF_3^+) and oxygen ion (O_2^+) bombardment, *Anal. Chem.* 59 (1987) 2081.
- [10] Y. Gao, H.N. Migeon, M. Juhel, J. Lecart, Enhanced SIMS analysis performance by CCl_4 flooding technique, *Surf. Interface Anal.* 20 (1993) 716.
- [11] J.M. McKinley, F.A. Stevie, T. Neil, J.J. Lee, L. Wu, D. Sieloff, C. Granger, Depth profiling of ultra-shallow implants using a Cameca IMS-6f, *J. Vac. Sci. Technol. B* 18 (2000) 514.
- [12] Victor K.F. Chia, Gary R. Mount, Michael J. Edgell, Charles W. Magee, Recent advances in secondary ion mass spectrometry to characterize ultralow energy ion implants, *J. Vac. Sci. Technol. B* 17 (1999) 2345.
- [13] M.H. Yang, G. Mount, I. Mowat, Ultrashallow profiling using secondary ion mass spectrometry: estimating junction depth error using mathematical deconvolution, *J. Vac. Sci. Technol. B* 24 (2006) 428.
- [14] M. Meuris, P. De Bisschop, J.F. Leclair, W. Vandervorst, Determination of the angle of incidence in a Cameca IMS-4f SIMS instrument, *Surf. Interface Anal.* 14 (1989) 739.
- [15] Jiang Zhi-Xiong, Paul F.A. Alkemade, Eelke Algra, S. Radelaar, High depth resolution SIMS analysis with low-energy grazing O_2^+ beams, *Surf. Interface Anal.* 25 (1997) 285.
- [16] M. Bernheim, G. Blaise, G. Slodzian, Sur la formation retardee d'ions a l'exterieur d'une cible soumise a un bombardement ionique, *Int. J. Mass Spectrom. Ion Phys.* 10 (1972) 293.
- [17] A.M. Lanzillotto, C.W. Magee, Electron stimulated desorption effects in secondary ion emission from BF_2^+ implanted SiO_2 , *J. Vac. Sci. Technol. A* 8 (1990) 983.
- [18] D.S. McPhail, M.G. Dowsett, E.H.C. Parker, Profile distortion during secondary ion mass spectrometry analyses of resistive layers due to electron stimulated desorption and charging, *J. Appl. Phys.* 60 (1986) 2573.
- [19] Berta Guzman de la Mat, DowettF Mark G., Ion and electron bombardment-related ion emission during the analysis of diamond using secondary ion mass spectrometry, *J. Appl. Phys.* 101 (2007) 034910-1.
- [20] J. Sielanko, J. Filiks, M. Sowa, J. Zinkiewicz, M. Drewniak, The freon flooding technique in SIMS analysis, *Vacuum* 46 (1995) 1459.
- [21] A. Corney, O.M. Williams, Measurement of the radiative lifetime of the 1S0 metastable level of atomic oxygen, *J. Phys. B: Atom. Mol. Phys.* 5 (1972) 686.
- [22] P.E. Siska, Molecular-beam studies of Penning ionization, *Rev. Mod. Phys.* 65 (1993) 337.
- [23] R.L. Sharpless, T.G. Slanger, Surface chemistry of metastable oxygen. II. Destruction of $\text{O}_2(a^1 \Delta_g)$, *J. Chem. Phys.* 91 (1989) 7947.
- [24] B. Carol Johnson, Peter L. Smith, R.D. Knight, The radiative lifetime of the $^5\text{S}_2^0$ metastable level of O^{++} , *Astrophys. J.* 281 (1984) 477.
- [25] K. Wittmaack, Current density effects in secondary ion emission studies, *Nucl. Instrum. Methods* 132 (1976) 381.
- [26] Hubert Gnaser, Singly- and doubly-negative carbon clusters in sputtering: energy abundance distributions and unimolecular fragmentation, *Nucl. Instrum. Methods Phys. Res. B* 149 (1999) 38.